Earthquake-induced displacements of gravity retaining walls and anchor-reinforced slopes

Aurelian C. Trandafir [a,*], Toshitaka Kamai [b], Roy C. Sidle [c]

[a] Department of Geology and Geophysics, University of Utah, 135 South 1460 East Rm 717, Salt Lake City, UT 84112-0111, USA
[b] Research Centre on Landslides, Disaster Prevention Research Institute, Kyoto University, Gokasho, Uji, 611-0011 Kyoto, Japan
[c] Slope Conservation Section, Geohazards Division, Disaster Prevention Research Institute, Kyoto University, Gokasho, Uji, 611-0011 Kyoto, Japan

ARTICLE INFO

ABSTRACT

This paper examines in terms of seismic performance, the effectiveness of anchor reinforcement against gravity retaining walls used to stabilize a dry homogenous fill slope in earthquake-prone environment. Both analyzed stabilizing measures have the same design yield acceleration estimated from a limit equilibrium approach. The earthquake-induced displacements are calculated using a sliding block formulation of the equation of motion. Sliding failure along the base of the gravity retaining wall and rotational failure of the soil active wedge behind the wall, as well as rotational failure of the slide mass of the anchor-reinforced slope were considered in the present formulation. For the specific characteristics of the analyzed fill slope and input horizontal ground motion, the slope reinforced with anchors appears to experience vertical and horizontal seismic displacements at slope crest smaller by 12% and respectively, 32% than the vertical and horizontal earthquake-induced deformations estimated at the top of the active wedge behind the gravity retaining wall.

© 2008 Elsevier Ltd. All rights reserved.

1. Introduction

Gravity walls are widely used as earth retaining systems supporting fill slopes adjacent to roads and residential areas built on reclaimed land. The October 23, 2004 Chuetsu earthquake, one of the largest recent seismic events in Japan, triggered numerous landslides across Niigata Prefecture; several residential developments constructed on reclaimed land in Nagaoka city incurred substantial damage to houses and roads due to earthquake-induced failure of artificial fill slopes [1,2]. Fig. 1 is a map of the damage in Takamachi-danchi residential area of Nagaoka city showing the zones affected by earthquake-induced fill slope failures. The tension cracks behind the gravity retaining walls supporting the fill material, and the zones of deformed and completely destroyed retaining walls (Fig. 1) were mapped during a post-earthquake field reconnaissance survey a few days after the Chuetsu earthquake, undertaken by an investigation team led by Prof. Toshitaka Kamai of the Disaster Prevention Research Institute, Kyoto University. The survey revealed that fill slope failures were caused by the excessive seismic displacements of the gravity retaining walls supporting the fill material (Fig. 2). The structural damage to houses and roads associated with earth-

quake-induced ground failure in Takamachi-danchi covered only those areas developed on fill slopes, whereas the structures located on natural slopes did not experience any visible damage during the Chuetsu earthquake.

During post-disaster investigations and discussions on potential mitigation measures related to the landslide damage in urban areas prone to earthquakes, the potential effectiveness of ground anchors to reinforce artificial fill slopes has been raised as an alternative to the existing gravity retaining walls. With the availability of modern execution technologies, reinforcement systems involving permanent grouted anchors may provide better technical and economical advantages compared to gravity retaining walls. This paper addresses the technical aspect of this problem by providing a comparative study on the seismic behavior of the two stabilization techniques (i.e., gravity retaining walls versus anchor reinforcements) applied to a dry homogeneous fill slope subjected to horizontal earthquake shaking. Both stabilizing measures are assumed to be designed at the same horizontal yield acceleration, which serves as basis of comparison for the calculated earthquake-induced displacements.

The dynamic displacement analysis presented in this study is based on the sliding block model originally developed by Newmark [3] to investigate the seismic behavior of earth structures. The sliding block approach has been extensively used in analyses of the seismic performance of slopes along rotational or planar failure surfaces in dry or saturated soils with or without

* Corresponding author. Tel.: +1 801 5850491; fax: +1 801 5817065.
E-mail addresses: atrandafir@yahoo.com, a.trandafir@utah.edu, atrandafir@earth.utah.edu (A.C. Trandafir).
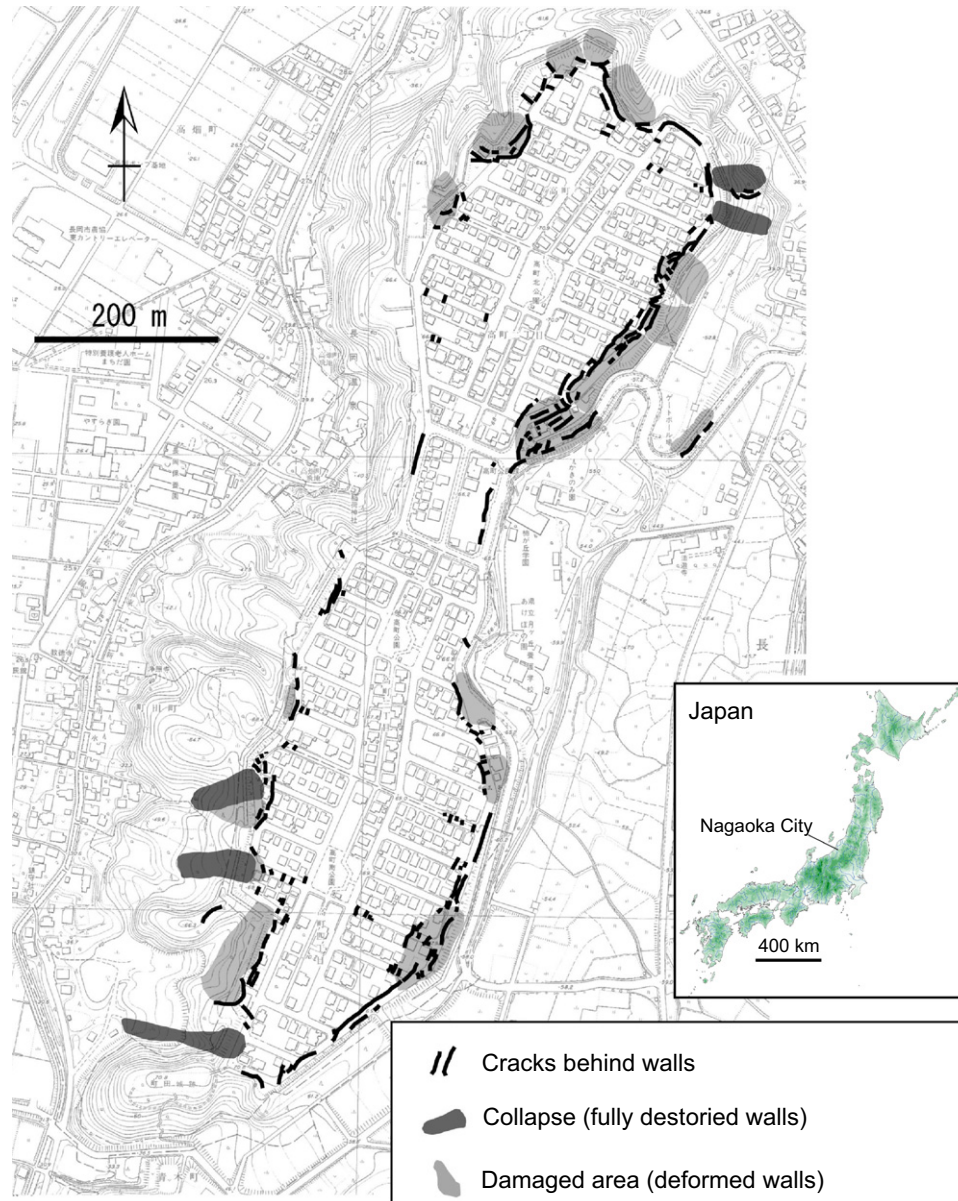
Takamachi-danchi, Nagaoka City

Fig. 1. Map of Takamachi-danchi residential area showing the ground failure and gravity retaining wall damage during the October 23, 2004 Chuetsu earthquake, Niigata, Japan.

degradation of yield strength along the sliding surface [4–14]. Richards and Elms [15] and Whitman and Liao [16] employed the Newmark procedure in evaluations of earthquake-induced displacements of gravity retaining walls, and Kim et al. [17] introduced a displacement approach for the seismic design of quay walls based on the sliding block concept. Applications of the Newmark model to the development of performance-based design charts for geosynthetic-reinforced slopes subjected to earthquake shaking have also been reported [18].

The Newmark model is basically a one-block translational or rotational mechanism along a rigid-plastic sliding surface, activated when the ground shaking acceleration exceeds a critical level. Therefore, this rigid block approach lacks the ability of modeling the seismic compliance of a soil slope or the dynamic response of backfill behind a retaining wall and, consequently, the associated effects on earthquake-induced displacements and dynamic wall thrust [2,19–23]. However, despite this deficiency, the Newmark sliding block concept is still widely used in

engineering practice even though finite-element commercial software is currently available for the analysis of the seismic behavior of earth retaining systems. One of the major shortcomings of a finite-element analysis when applied to rigorous predictions of permanent deformations is the requirement for sophisticated nonlinear elasto-plastic models that should be able to account for the nonlinear inelastic behavior of the soil and of the interfaces between the soil and the wall elements. The parameters characterizing these constitutive models are derived from specialized laboratory tests that are not readily available to the practitioners. Furthermore, numerical instabilities may easily occur in finite-element computations due to significant distortions of the finite-element mesh in order to achieve relatively moderate to large permanent deformations. Dynamic finite-element meshes that would regenerate with progressive deformation to avoid excessive distortions are still in a development stage and have not yet been implemented in commercial software. For such reasons, the sliding block model still represents an attractive

option when performing quantitative preliminary assessments of earthquake-induced permanent displacements, since it requires only fundamental design information (e.g., geometry of the problem), a minimum number of material properties (i.e., unit weight and shear strength parameters), and involves a robust computational process.

2. Sliding block formulation for fill slope supported by gravity wall

The geometry of the analyzed fill slope and gravity retaining wall is presented in Fig. 3 as a typical cross section from Takamachi-danchi residential area of Nagaoka city, Niigata Prefecture, Japan, which was severely damaged by the October 23, 2004 Chuetsu earthquake (Figs. 1 and 2). A retaining wall of height $H_w = 5.4$ m is used to hold back the earth and maintain a

Fig. 2. Gravity retaining wall in Takamachi-danchi residential area damaged during the October 23, 2004 Chuetsu earthquake, Niigata, Japan.

difference in the elevation of the ground surface which has a height $H = 7.6$ m from the wall base. The case of a dry homogeneous fill is considered herein with a unit weight $\gamma = 17$ kN/m^3, an internal angle of friction $\phi = 27°$ and a cohesion $c = 10$ kPa. The gravity retaining wall (Fig. 3) has a base friction angle $\phi_b = 28°$, and a unit weight $\gamma_b = 23$ kN/m^3 yielding a wall weight $W_w = 220.4$ kN.

The forces shown in Fig. 3 are the weight (W_w) and the horizontal inertia force (kW_w) of the gravity retaining wall, the weight (W) and the horizontal inertia force (kW) of the active soil wedge behind the wall, and the normal (N_w) and resistant (T_w) forces along the base of gravity retaining wall. The forces acting on an individual soil column of width dx within the active wedge (Fig. 3) are the normal (N) and resistant (T) forces along the base of the column, the column weight (dW), the inertia force of the column (k(dW)), the left side vertical (V_L) and horizontal (X_L) forces, and the right side vertical (V_R) and horizontal (X_R) forces. In Fig. 3, α represents the angle of the column base with horizontal, and $\beta = 6°$ is the inclination angle of the back of the wall to vertical. Parameter k in the expression of inertia forces represents the coefficient of horizontal earthquake acceleration (Fig. 3).

2.1. Assumptions

Similar with Richards and Elms [15], the basic assumption of the analysis is that the retaining wall and the soil active wedge behind the wall (Fig. 3) act as rigid bodies, and during motion, the shear strength is fully mobilized along the base of the wall, as well as along the failure surface of the active wedge. As illustrated in Fig. 4, a base sliding mechanism associated with translational failure is considered for the analyzed gravity retaining wall. This assumption conforms to the situation in Takamachi-danchi area where field investigations indicate a stiff foundation soil underlying the gravity retaining walls [2]. Furthermore, additional examinations of failed gravity retaining walls in Takamachi-danchi area after the October 23, 2004 Chuetsu seismic event, revealed significant translational wall movements during the earthquake. For the active soil wedge behind the wall, a rotational failure mechanism along a circular slip surface is considered
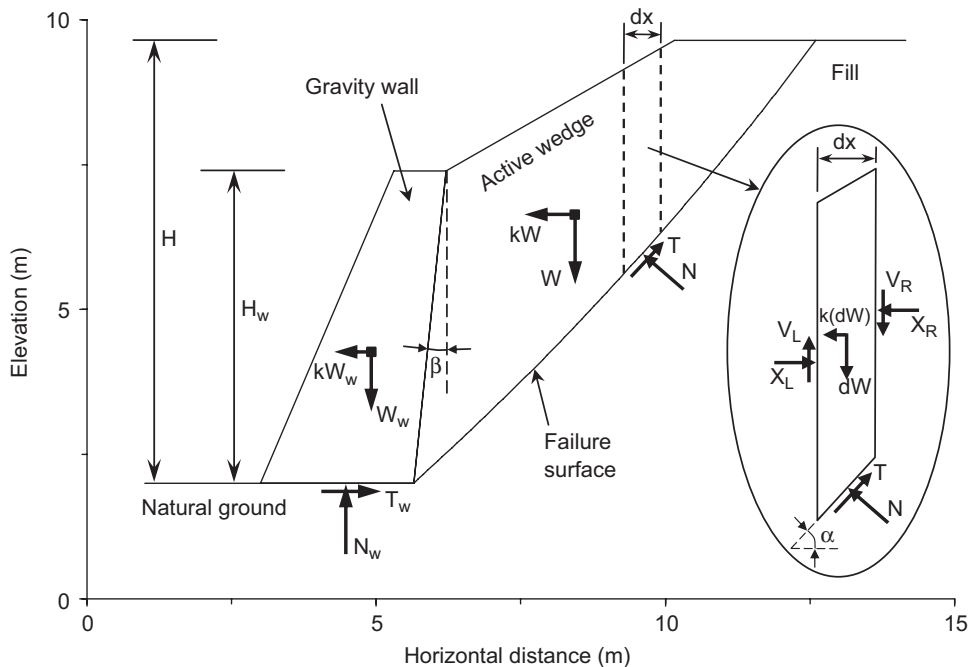

Fig. 3. Forces considered in the seismic sliding block analysis of the gravity retaining wall–active wedge system.
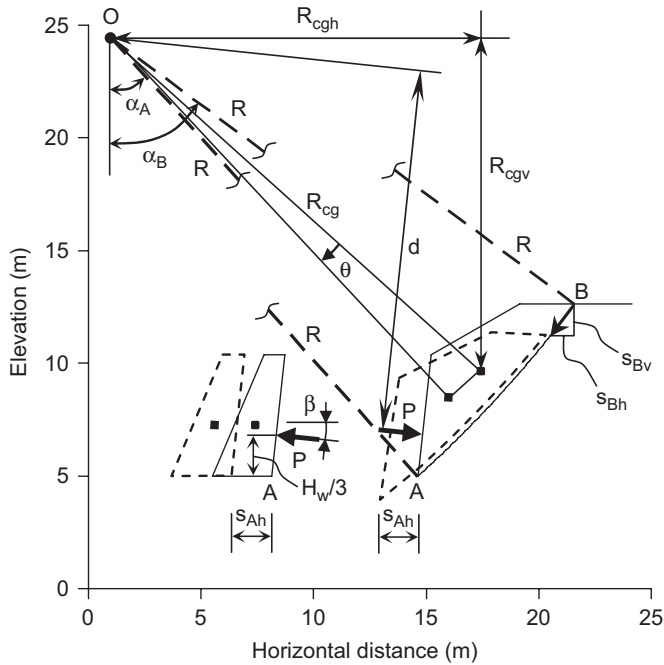
Fig. 4. Illustration of the translational failure mechanism for the gravity retaining wall, and the rotational failure mechanism for the potential sliding soil mass within the fill slope.

(Fig. 4). As shown later in this paper, the same type of rotational failure will also be considered for the slide mass of the fill slope reinforced with anchors. Hence, a unique failure mechanism adopted for both categories of sliding soil masses (i.e., active wedge behind a gravity retaining wall and failure mass of an anchor-reinforced slope) enables us to perform a comparison of the earthquake-induced displacements associated with the two stabilization techniques (i.e., gravity retaining walls and anchors) investigated in this study.

Another assumption made in the analysis is that during the earthquake, wall displacements occur only outwards (or away) from the backfill, and the active wedge experiences only down-slope movement (Fig. 4). This assumption is reasonable for most cases encountered since very high yield accelerations must be exceeded by the ground shaking acceleration in order to cause wall movements towards the backfill and upslope displacements of the sliding soil wedge (which in this case would become a passive wedge) behind the wall.

In the present investigation, a smooth wall–backfill interface is considered, implying that the wall thrust P acts normal to the wall–backfill interface, therefore, making an angle β with the horizontal (Fig. 4). The height of the line of action for thrust P is taken as $H_w/3$ from the wall base (Fig. 4), and assumed to not vary during the earthquake. Although this is not the real case, it will be demonstrated later that for the objective of the particular analyzed problem, this assumption is quite reasonable. Finally, the assumption that the retaining wall and the active wedge are in permanent contact during motion involves $P > 0$ during the earthquake shaking. This condition will also be examined later in the paper.

2.2. Equation of motion

The parameter of motion for the gravity retaining wall with a basal sliding mechanism is the horizontal displacement s_{Ah} of point A defining the bottom-right corner of the wall in Fig. 4. Referring to the forces shown in Figs. 3 and 4, the relative

acceleration $\ddot{s}_{Ah}$ of the retaining wall may be derived from the Newton's second law of motion on the horizontal direction:

$$\frac{W_w}{g}\ddot{s}_{Ah} = P\cos\beta + kW_w - T_w, \tag{1}$$

where g represents the gravitational acceleration.

At sliding, the frictional resistance developed along the wall base is fully mobilized, thus

$$T_w = N_w\tan\phi_b = (W_w - P\sin\beta)\tan\phi_b. \tag{2}$$

By substituting T_w in Eq. (1) with the expression given in Eq. (2), and rearranging Eq. (1), we obtain

$$\ddot{s}_{Ah} = \left[\frac{P}{W_w}\frac{\cos(\phi_b-\beta)}{\cos\phi_b} + k - \tan\phi_b\right]g. \tag{3}$$

For the rotational failure mechanism depicted in Fig. 4, the parameter of motion of the active wedge behind the retaining wall is the rotation θ of the center of gravity about the pole O of the slip circle. The angular acceleration of the active wedge ($\ddot{\theta}$) is derived from the difference between the driving moment (given by forces kW, W and P) and the resisting moment (given by resistant force T along failure surface) about the pole O of the slip circle (Figs. 3 and 4):

$$\frac{W}{g}R_{cg}^2\ddot{\theta} = kWR_{cgv} + WR_{cgh} - Pd - R\sum T, \tag{4}$$

where R_{cg} represents the distance from the pole of the slip circle to the center of gravity of the active wedge, R_{cgv} and R_{cgh} are the vertical and horizontal projections of R_{cg}, d is the perpendicular distance from the pole of the slip circle to the line of action of wall thrust P, and R is the radius of the slip circle. During motion, the available soil shear strength is fully mobilized along the sliding surface, thus the resistant force (T) at the base of an individual soil column within the active wedge (Fig. 3) is given by the Mohr–Coulomb failure criterion

$$T = N\tan\phi + \frac{c\,dx}{\cos\alpha}. \tag{5}$$

By making the assumption that $V_L = V_R = 0$ as in Bishop's simplified method of slices for slope stability analysis, the normal force (N) can be derived from the vertical force equilibrium equation of the soil column (Fig. 3):

$$N\cos\alpha + T\sin\alpha - dW = 0. \tag{6}$$

Eqs. (5) and (6) lead to an explicit expression of T for each individual column within the active wedge, which can be used to estimate the quantity ΣT in Eq. (4) representing the total resistant force developed along the failure surface.

As shown in Fig. 4, point A on the gravity retaining wall and point A at the bottom of the active wedge have the same horizontal displacement, hence the motion parameters s_{Ah} and θ can be linked by the following equation:

$$s_{Ah} = R\theta\cos\alpha_A, \tag{7}$$

where α_A is the angle with the horizontal made by the tangent at the failure surface in point A (of the active wedge). A similar form of Eq. (7) may be obtained in terms of accelerations ($\ddot{s}_{Ah}$ and $\ddot{\theta}$), which combined with Eqs. (3) and (4) renders the following expression:

$$\frac{\ddot{\theta}}{g}\left[W\frac{R_{cg}^2}{d} + W_w\frac{\cos\phi_b}{\cos(\phi_b-\beta)}R\cos\alpha_A\right] = k\left[W\frac{R_{cgv}}{d}\right.$$
$$\left. + W_w\frac{\cos\phi_b}{\cos(\phi_b-\beta)}\right] + \left[W\frac{R_{cgh}}{d} - W_w\frac{\sin\phi_b}{\cos(\phi_b-\beta)} - \frac{R}{d}\sum T\right]. \tag{8}$$

Based on Eq. (8), the closed-form solution of the angular acceleration can be obtained:

$$\ddot{\theta} = C_w(a - k_y g), \tag{9}$$

where a represents the earthquake acceleration ($a = kg$), k_y designates the yield coefficient of the retaining wall–active wedge system, and C_w is a constant defined as

$$C_w = \frac{W(R_{cgv}/d) + W_w(\cos\phi_b/\cos(\phi_b - \beta))}{W(R_{cg}^2/d) + W_w(\cos\phi_b/\cos(\phi_b - \beta))R\cos\alpha_A}. \tag{10}$$

When an increasing earthquake acceleration reaches the value of yield acceleration (k_yg) no displacement occurs but the shear strength developed along the base of the retaining wall and the failure surface of the active wedge is fully mobilized, i.e., the retaining wall–active wedge system is in a state of limit equilibrium. The yield coefficient (k_y) can be easily obtained from Eq. (8) by setting $\ddot{\theta} = 0$ and $k = k_y$. The expression of k_y derived in this manner together with Eqs. (5) and (6) can be incorporated into a computer code, and an automatic search procedure can be employed to locate the critical failure surface of the active wedge associated with the minimum value of k_y. In this study, however, another approach will be used to determine k_y, as described in the next section.

The step by step numerical integration procedure to calculate the permanent rotation (θ) induced by a seismic excitation, given the expression of the angular acceleration, is described in detail elsewhere [12]. Based on the value of θ at the end of earthquake shaking, the vertical and horizontal permanent displacements of point B at the top of the active wedge in Fig. 4 can be determined by the equations below:

$$s_{Bv} = R\theta\sin\alpha_B, \tag{11}$$

$$s_{Bh} = R\theta\cos\alpha_B, \tag{12}$$

where s_{Bv} and s_{Bh} are the vertical and horizontal displacements of point B in Fig. 4, and α_B is the angle with the horizontal made by the tangent at the failure surface in point B (Fig. 4). The relative acceleration of the wall derived from Eqs. (7) and (9) is

$$\ddot{s}_{Ah} = (a - k_yg)C_wR\cos\alpha_A. \tag{13}$$

2.3. Yield coefficient

In their analysis of earthquake-induced gravity retaining wall displacements, Richards and Elms [15] suggested that the yield acceleration of wall–backfill system can be evaluated from the limit equilibrium of the retaining wall using the equation of active wall thrust (P) derived from a Mononobe–Okabe analysis. Due to the presence of seismic coefficient (k) in the expression of dynamic wall thrust given by Mononobe–Okabe approach, an iterative procedure is required to determine the yield acceleration, as described by Kramer [24]. In this study, however, a graphical procedure is used to evaluate the yield coefficient (k_y) using the values of active wall thrust (P) estimated separately for the gravity retaining wall and the soil active wedge behind the wall (Fig. 4) from the condition of limit equilibrium of each of the two bodies at various seismic coefficients (k).

The equation of wall thrust (P) for the gravity retaining wall at limit equilibrium is obtained from Eq. (3) for $\ddot{s}_{Ah} = 0$:

$$P = \frac{W_w\cos\phi_b}{\cos(\phi_b - \beta)}(\tan\phi_b - k), \tag{14}$$

where P is a linear function of k in Eq. (14), and the graphical representation of this relationship is given in Fig. 6 for the characteristics of the analyzed gravity retaining wall (Fig. 3).

The P–k relationship at limit equilibrium for the active wedge behind the wall, which is depicted in Fig. 6, was derived from a pseudostatic slope stability analysis based on Bishop's simplified method (Fig. 5). For this purpose, the limit-equilibrium based

commercial software SLOPE/W of the GEO-SLOPE OFFICE package [25] was employed. According to the basic principle in a limit-equilibrium based slope stability approach, the seismic coefficient (k) that would bring the potential slide mass in limit equilibrium for a given wall thrust (P) is the coefficient of pseudostatic seismic force (kW) associated with a safety factor (FS) of 1.0. Thus for each assumed P value, k was gradually increased and the safety factor was calculated until the value of k corresponding to $FS = 1.0$ was found. For each pair of analyzed (P, k) values, the minimum factor of safety (FS) was determined by enabling the automatic search option in SLOPE/W to locate the pole of the critical failure surface across a grid of potential slip circle centers. Fig. 5 depicts some of the P and corresponding k values at limit equilibrium (i.e., $FS = 1.0$) together with the associated critical slip surfaces obtained from slope stability analyses based on Bishop's simplified method by utilizing the described procedure.

The intersection point of the P–k relationships at limit equilibrium established for the gravity retaining wall and the active soil wedge behind the wall (Fig. 6) renders the yield coefficient (k_y) of the wall–backfill system. Any other k value different from k_y produces different limit-equilibrium values of P on the gravity wall and the active wedge (Fig. 6), thus contradicting the physical meaning of wall thrust—i.e., an internal force with equal magnitude on either of the two contact elements (Fig. 4). The yield coefficient and the associated thrust of the analyzed gravity wall–active wedge system (Fig. 3) is $k_y = 0.148$ and $P = 80.5$ kN, as obtained from the graphical analysis depicted in Fig. 6. The critical failure surface of the active wedge for this set of (P, k) values is illustrated in Figs. 3 and 5, and the associated geometrical features (Fig. 4) are $R = 51.13$ m, $R_{cg} = 49.82$ m, $R_{cgv} = 33.43$ m, $R_{cgh} = 36.94$ m, $d = 32.51$ m, $\alpha_A = 41.9°$, $\alpha_B = 53.5°$, yielding a weight of the active wedge $W = 359.8$ kN.

Alternatively, the limit-equilibrium P–k relationship of the active wedge behind the wall was estimated from a Mononobe–Okabe analysis (Fig. 6). As shown in Fig. 7, the Mononobe–Okabe
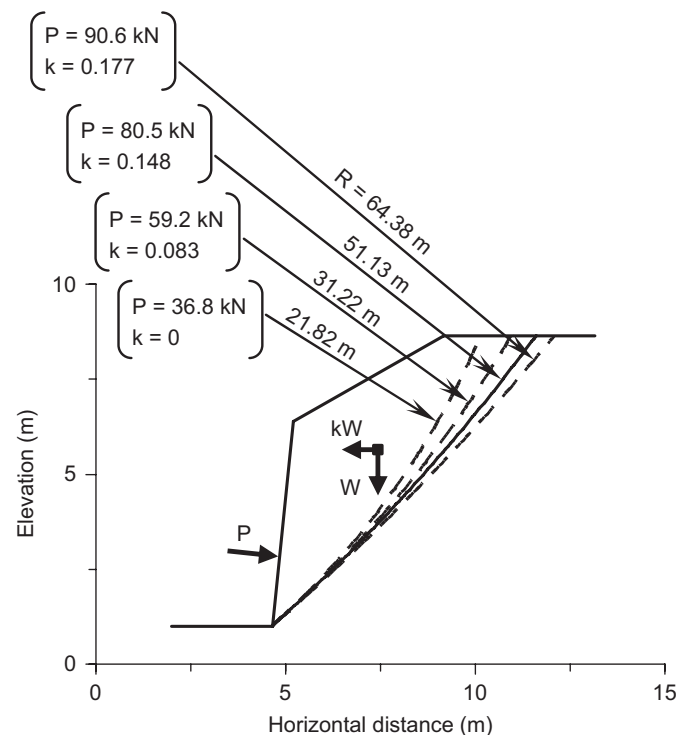
Fig. 5. Critical circular slip surfaces for various magnitudes of dynamic wall thrust (P) and corresponding seismic coefficients (k) at limit equilibrium of the active wedge (i.e., $FS = 1.0$).

approach considers the limit equilibrium of an active wedge delineated by a planar failure surface making an angle α^* with the horizontal. Although closed-form solutions based on Mononobe–Okabe's method are available in the literature for the active wall thrust (P) of a triangular wedge with a uniform backfill gradient [26,27], such expressions cannot be applied to the particular geometry of the analyzed active wedge with variable gradient at the backfill surface (Fig. 7). Therefore, the equation yielding the wall thrust P was derived from the vertical and horizontal equilibrium of forces acting on the active wedge (Fig. 7) coupled with the Mohr–Coulomb failure criterion (i.e., Eq. (5) in which $dx = H/\tan \alpha^*$):

$$P^{Mononobe-Okabe} = \frac{W[k\cos(\alpha^* - \phi) + \sin(\alpha^* - \phi)] - cH\cos\phi/\sin\alpha^*}{\cos(\beta + \alpha^* - \phi)}.$$

(15)

The P–α^* relationships represented in Fig. 7 were obtained based on Eq. (15), for various specific values of the seismic coefficient (k). The points defining the peak of these relationships provide the

active wall thrust (P) and the inclination α^*_{cr} of the critical failure plane. The peak P values were plotted against the corresponding k values in Fig. 6, generating the P–k relationship at limit equilibrium for the active wedge based on Mononobe–Okabe approach.

The analysis based on Bishop's simplified method to derive the P–k relationship in Fig. 6 may be conservative when compared to the Mononobe–Okabe analysis since for the same seismic coefficient, Bishop's method produces greater P values required for the limit equilibrium of the active wedge. However, the difference in the active wall thrust derived from these two methods appears to decrease with the increase in the seismic coefficient (Fig. 6). This behavior is closely related to the shape of the critical sliding surface derived from the Bishop analysis. As noted in Fig. 5, the curvature ($1/R$) of the critical slip circle at limit equilibrium decreases as k increases, indicating that the shape of the critical sliding surface is approximating a planar surface. Hence, for higher seismic coefficients, the Mononobe–Okabe's planar failure mechanism becomes predominant. At $k = k_y$, the difference in P values estimated from Bishop and Mononobe–Okabe analyses becomes practically insignificant (Fig. 6). Thus, for the analyzed problem, both approaches produce essentially the same yield acceleration of the wall–backfill system.

Experimental and numerical studies on the location of dynamic wall thrust (P) across the wall height indicate that the resultant of dynamic earth pressure during an earthquake may reach heights equal to $H_w/2$ from the bottom of the wall [28–31]. For a height $H_w = 5.4\,m$ corresponding to the wall depicted in Fig. 3, a variation in the height of the line of action of P within $H_w/2$–$H_w/3$ translates into less than 3% variations of distance d in Eqs. (4) and (8), which can therefore be ignored. Hence, the assumption made in our study that during earthquake, P acts at a constant height equal to $H_w/3$ from the wall base (Fig. 4) appears reasonable.

Addressing the seismic behavior of gravity retaining walls, Richards and Elms [15] calculated the earthquake-induced relative wall displacements by simply integrating the portions of earthquake acceleration time history above the yield acceleration of the wall–backfill system. In such a case, the relative wall acceleration is ($a-k_yg$). In Eq. (13), we arrive at the same expression of relative wall acceleration if $C_wR\cos\alpha_A = 1.0$, a condition achieved for $W = 0$ in Eq. (10) which may be interpreted as the active wedge playing no role in the relative wall acceleration. For the analyzed wall–backfill system (Fig. 3), the constant $C_wR\cos\alpha_A$ is 0.622, therefore representing a reduction factor for the quantity ($a-k_yg$).
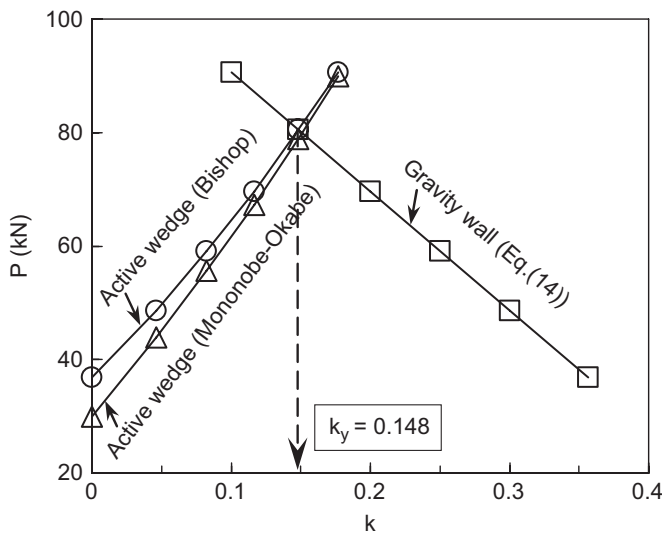

Fig. 6. Graphical procedure to determine the yield coefficient (k_y) of the gravity wall–backfill system based on the P–k relationships at limit equilibrium established independently for the gravity retaining wall and the soil active wedge behind the wall.
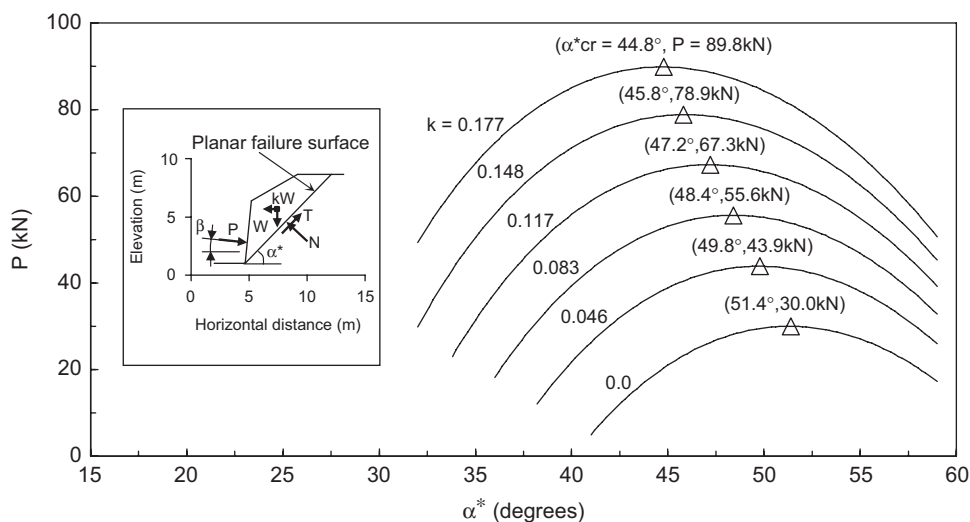

Fig. 7. Mononobe–Okabe analysis to evaluate the dynamic wall thrust (P) and inclination of critical failure plane (α^*_{cr}) for different seismic coefficients (k).

This reduction factor is directly related to the variation of inertia force acting on the active wedge (and consequently the variation in wall thrust P) associated with relative motion (i.e., $R_{cg}\ddot{\theta}$) of the wedge during an earthquake; an aspect which appears to be neglected in the integration procedure utilized by Richards and Elms [15].

The equation of motion derived for the wall–backfill system in the previous section is based on the assumption that the gravity wall and the active wedge (Fig. 3) are in permanent contact, implying that the wall thrust (P) has a positive value during the entire motion process. To verify this condition, the expression of P during motion was obtained using Eqs. (3) and (13), as follows:

$$P = \frac{W_w \cos \phi_b}{\cos(\phi_b - \beta)}[\tan \phi_b - k_y C_w R \cos \alpha_A - k(1 - C_w R \cos \alpha_A)]. \quad (16)$$

According to Eq. (16), the condition $P > 0$ translates into

$$k < \frac{\tan \phi_b - k_y C_w R \cos \alpha_A}{1 - C_w R \cos \alpha_A}, \quad (17)$$

which for the analyzed problem becomes $k < 1.163$. Eq. (17) indicates that for ground shaking accelerations greater than 1.163g, the gravity retaining wall may detach from the active wedge and move independently during motion. Consequently for $a > 1.163g$, Eqs. (7)–(10) and (13) are no longer valid. In this study, however, the range of considered peak earthquake accelerations does not exceed 1g, therefore the condition $P > 0$ is achieved for the analyzed input earthquake.

3. Sliding block formulation for fill slope reinforced with anchors

3.1. Assumptions

In Fig. 8, the dry homogeneous fill slope (Fig. 3) is assumed to be reinforced with one row of grouted anchors, which represents the other case examined in this study. The anchor reinforcement mechanism consists basically of transferring the resisting tensile force P of the anchor into the ground through the friction mobilized at the soil–grout interface. The load P developed in anchor is due to the earth pressure exerted against the structural facing (e.g., bearing plates, concrete pad or tensioned geosynthetics) to which the anchors are connected and eventually prestressed. As seen in Fig. 8, the anchors are considered to be

Fig. 8. Forces considered in the seismic sliding block analysis of the anchor-reinforced slope.

installed at a height $H_w/2$ from the bottom of the slope across the steep slope gradient, and driven into the ground at an inclination angle β with the horizontal ($H_w = 5.4$ m and $\beta = 6°$ from Fig. 3).

The same assumptions and rotational failure mechanism considered for the active wedge behind the gravity retaining wall (Figs. 3 and 4) are adopted for the potential sliding soil mass of the anchor-reinforced slope (Fig. 8). Regarding the anchor, it is assumed that the shear resistance developed along the soil–grout interface is fully mobilized during motion. Also, the potential variations in the shear resistance of the soil–grout interface that may arise due to changes in normal stress during earthquake are neglected, as well as the potential shear stresses that may develop along the sliding surface (at the intersection point between the anchor and slip surface) due to deformation of the anchor tendon associated with the seismic displacement of failure mass. These assumptions lead to a constant anchor load P equal to the pullout resistance of reinforcement per unit length.

3.2. Equation of motion

For the rotational failure mechanism along a circular slip surface (depicted in Fig. 4), the angular acceleration of the sliding soil mass of anchor-reinforced slope (Fig. 8) is derived from Eq. (4) in which P is the reinforcement load, d is the perpendicular distance from the pole of the slip circle to the line of reinforcement, and T is derived from Eqs. (5) and (6). Based on Eq. (4), a solution similar to the expression given in Eq. (9) for the gravity wall–backfill system is obtained for the angular acceleration ($\ddot{\theta}$) of the anchor-reinforced slope:

$$\ddot{\theta} = C_a(a - k_y g), \quad (18)$$

where C_a is a constant defined as

$$C_a = \frac{R_{cgv}}{R_{cg}^2}. \quad (19)$$

Eq. (18) is the same as the solution of the angular acceleration provided by Ling and Leshchinsky [12] for simple slopes with the sliding mass treated as a rigid rotating body defined by a log spiral slip surface. The expression of the yield coefficient (k_y) in Eq. (18) can be derived from Eq. (4) by setting $\ddot{\theta} = 0$ and $k = k_y$.

3.3. Yield coefficient

In order to be able to perform a comparison of the permanent seismic displacements for the two earth retaining systems analyzed in this study, the anchor-reinforced slope (Fig. 8) was assumed to be designed at the same yield coefficient as the gravity retaining wall–backfill system (Fig. 3), i.e., $k_y = 0.148$, and the associated reinforcement load P was estimated from a pseudostatic slope stability analysis based on Bishop's simplified method using the limit-equilibrium software SLOPE/W [25]. The reinforcement load option and the automatic search procedure for locating the center of the critical slip surface across a grid of trial slip circle centers were used in the SLOPE/W calculations. Following the fundamental principle of limit-equilibrium slope stability analysis, the reinforcement load P corresponding to a specific design yield coefficient k_y was determined by considering various magnitudes of force P and calculating the safety factor (FS) for a pseudostatic horizontal seismic force $kW = k_yW$ (Fig. 8) until the P value associated with $FS = 1.0$ was obtained. For a design yield coefficient $k_y = 0.148$ of the anchor-reinforced slope in Fig. 8, the reinforcement load derived from such an analysis is $P = 82.9$ kN, and the corresponding geometrical characteristics (Fig. 4) of
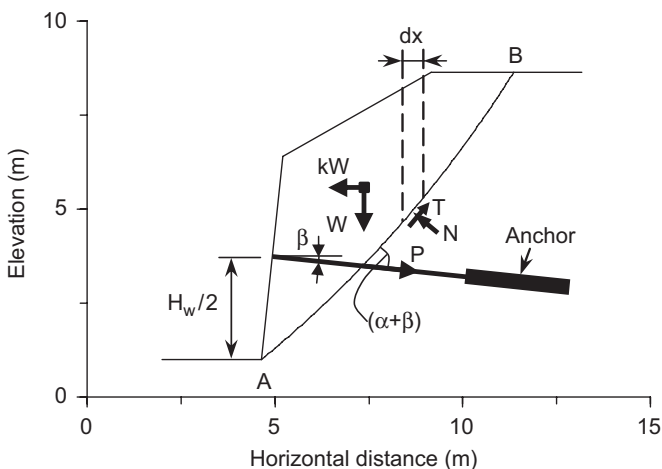
the critical failure surface (illustrated in Fig. 8) and sliding soil mass are $R = 31.75$ m, $R_{cg} = 30.39$ m, $R_{cgv} = 19.94$ m, $R_{cgh} = 22.94$ m, $d = 19.57$ m, $\alpha_A = 39.5°$, $\alpha_B = 57.9°$, yielding a weight of sliding soil mass $W = 360.4$ kN.

In *SLOPE/W* analysis involving soil reinforcements such as anchors, the reinforcement load is treated as a line load acting at the intersection point between the line of reinforcement and the failure surface [25]. Hence, the vertical equilibrium of forces (used to derive the normal force N at the base of the slice) in a Bishop's simplified approach, for the slice containing the reinforcement load P (Fig. 8), includes the vertical component of force P (i.e., $P\sin\beta$) in addition to the forces in Eq. (6):

$$N\cos\alpha + T\sin\alpha - dW - P\sin\beta = 0. \qquad (20)$$

This approach (adopted in *SLOPE/W*) is denoted as the "conventional approach" in this paper.

Recently, Cai and Ugai [32] investigated the conventional approach regarding the mechanism of anchor reinforcement in slopes by examining the static safety factors obtained from a series of slope stability analyses using finite-element method and limit-equilibrium based Bishop's simplified method. Their study demonstrated that in fact, the component of reinforcement load tangent to the sliding surface (i.e., $P\cos(\alpha+\beta)$) does not affect the normal force N at the base of the slice containing the reinforcement load P (Fig. 8). Consequently, the effect of anchor reinforcement in Eq. (20) will be given solely by the vertical projection of that component of reinforcement load P acting normal on the sliding surface (i.e., $P\sin(\alpha+\beta)$):

$$N\cos\alpha + T\sin\alpha - dW - P\sin(\alpha+\beta)\cos\alpha = 0. \qquad (21)$$

This anchor reinforcement approach proposed by Cai and Ugai [32] is denoted herein as the "modified approach".

To account for the modified reinforcement approach in *SLOPE/W* stability analysis of the anchor-reinforced slope shown in Fig. 8, the equivalent system of forces (P_1, T_a) is considered, as shown in Fig. 9. Both forces act at the intersection point between line of reinforcement and sliding surface (Fig. 9). Force P_1 is the reinforcement load in the *SLOPE/W*'s conventional approach, which in combination with the tangential force T_a, produces the same effect as the reinforcement load P (Fig. 8) in the modified approach. Accordingly, for the Bishop's simplified method, the moment given by forces P_1 and T_a about the pole of the circular slip surface (Fig. 4) must be equal to the moment of reinforcement load P, and the vertical component of the resultant force generated by P_1 and T_a must be equal to the vertical projection of the normal component of reinforcement load $P\sin(\alpha+\beta)$. These conditions translate into

$$P_1\cos(\alpha+\beta) + T_a = P\cos(\alpha+\beta), \qquad (22)$$

$$P_1\sin\beta - T_a\sin\alpha = P\sin(\alpha+\beta)\cos\alpha. \qquad (23)$$

Based on Eqs. (22) and (23), the following relationship between P_1 and T_a is obtained:

$$T_a = P_1 \frac{\cos(\alpha+\beta)}{\sin(2\alpha+\beta)}[\sin\beta - \sin(\alpha+\beta)\cos\alpha]. \qquad (24)$$

In the pseudostatic slope stability analysis using *SLOPE/W*, various magnitudes of forces P_1 and corresponding T_a (as given by Eq. (24)) were considered and safety factors (*FS*) were calculated. The P_1 and T_a forces that produce a safety factor $FS = 1.0$ for a pseudostatic horizontal seismic force kW (Fig. 8) corresponding to the design yield coefficient $k_y = 0.148$, are $P_1 = 113.5$ kN and $T_a = -31.4$ kN (the negative sign indicates that T_a acts in a direction opposite to that shown in Fig. 9). The characteristics of the critical slip surface and sliding soil mass (Fig. 4) in this case are $R = 26.24$ m, $R_{cg} = 24.85$ m, $R_{cgv} = 16.09$ m, $R_{cgh} = 18.94$ m, $d = 16.11$ m, $\alpha_A = 38.2°$, $\alpha_B = 60.4°$, and the corresponding weight of sliding soil mass is $W = 360.2$ kN. The reinforcement load P in the modified approach estimated using Eq. (22) is 62.7 kN, about 24% smaller than the reinforcement load determined using the conventional reinforcement approach (i.e., $P = 82.9$ kN).

4. Seismic displacements

The sliding block formulations developed in the previous sections were used to study the seismic performance of the analyzed gravity retaining wall–backfill system (Fig. 3) and anchor-reinforced slope (Fig. 8) for the input horizontal earthquake given in Fig. 10. The accelerogram was recorded during the October 23, 2004 Chuetsu earthquake at a station located approximately 1.8 km northeast of Takamachi-danchi, a residential area of Nagaoka city, Niigata Prefecture, Japan, which suffered severe landslide damage during the earthquake (Figs. 1 and 2). Positive values on the accelerogram in Fig. 10 are associated in this analysis with horizontal inertia forces due to the earthquake (kW and kW_w) acting as shown in Figs. 3 and 8.

Fig. 11 shows the evolution of earthquake-induced vertical and horizontal displacements (s_{Bv} and s_{Bh}) at point B on the top of the active wedge behind the wall in Fig. 4, and point B on the top of the sliding mass of the anchor-reinforced slope in Fig. 8. The displacements were estimated based on Eqs. (11) and (12) using the calculated rotation (θ) of the slide mass at a certain instant during earthquake. For the anchor-reinforced slope, the characteristics of critical failure mass determined from pseudostatic stability analyses based on both conventional and modified reinforcement approaches (as discussed in Section 3.3) were used in dynamic calculations (Fig. 11). As seen in Fig. 11, the difference in calculated seismic displacements when comparing the two reinforcement approaches is practically insignificant. Hence, even though the conventional reinforcement approach may seriously
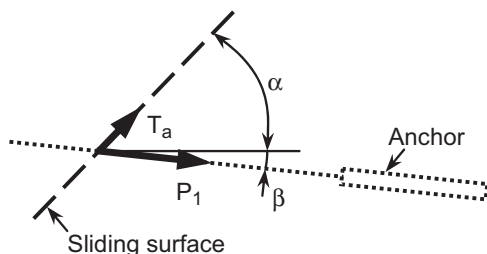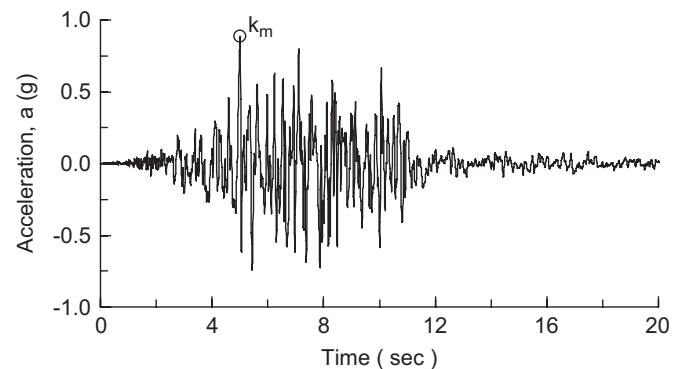

Fig. 9. Equivalent system of forces considered in the pseudostatic *SLOPE/W* stability analysis of the anchor-reinforced slope to account for the modified reinforcement approach.

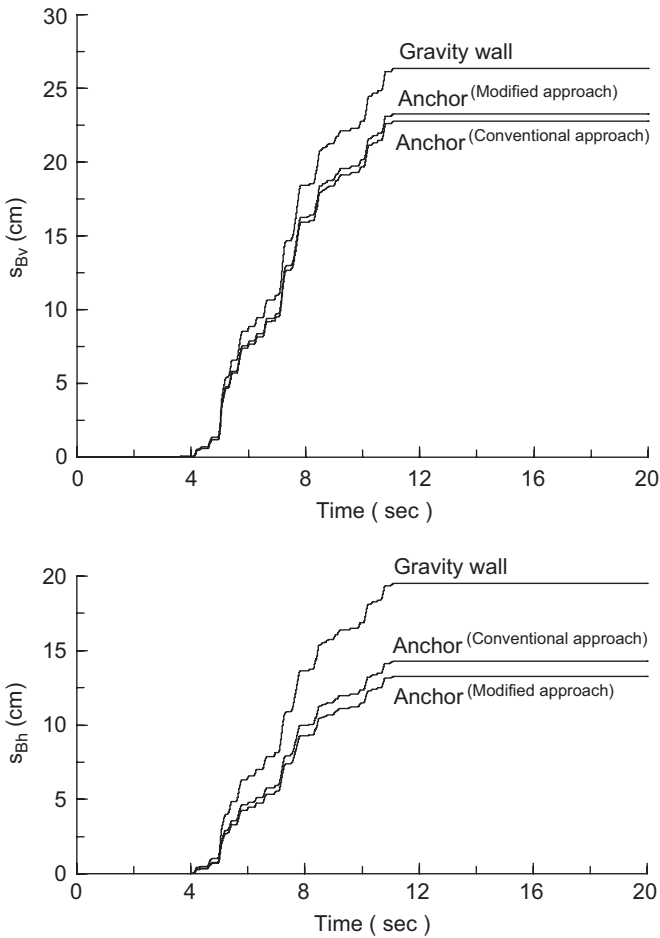

Fig. 10. Input horizontal ground motion.

Fig. 11. Evolution of vertical (s_{Bv}) and horizontal (s_{Bh}) displacements during earthquake at the top of the sliding soil mass within the fill slope supported by gravity retaining wall or reinforced with anchors.

Fig. 12. Permanent vertical (s_{Bv}) and horizontal (s_{Bh}) seismic displacements at the top of the sliding soil mass within the fill slope supported by gravity retaining wall or reinforced with anchors, in relation to the peak earthquake acceleration coefficient (k_m).

overestimate the reinforcement load required for a specific design yield coefficient (as shown in Section 3.3), this approach can still provide reasonable estimates of earthquake-induced displacements of a slope reinforced with anchors. Overall, the data in Fig. 11 indicate larger seismic displacements of the active wedge behind the wall (Figs. 3 and 4) when compared to the anchor-reinforced slope (Fig. 8) despite the same design yield coefficient of the two sliding systems. This result demonstrates the significant role played in the relative motion by the inertia force imparted on the gravity retaining wall due to the earthquake loading (kW_w).

The diagrams depicted in Fig. 12 were obtained by scaling the input seismic record to different values of peak earthquake acceleration (k_m in Fig. 10) and computing the corresponding earthquake-induced permanent vertical and horizontal displacements (s_{Bv}^p and s_{Bh}^p) at point B on the top of active wedge behind the wall (Fig. 4) and point B on the top of sliding mass of the anchor-reinforced slope (Fig. 8). A nonlinear relationship between the permanent displacement and the peak earthquake acceleration coefficient characterizes all cases analyzed in Fig. 12. Again, the results indicate an insignificant difference between permanent displacements of the anchor-reinforced slope evaluated using the characteristics of critical failure mass associated with the conventional and modified reinforcement approaches discussed in Section 3.3. On the other hand, the difference between the permanent displacement of the active wedge behind the gravity retaining wall (Fig. 4) and the permanent displacement of the anchor-reinforced slope (Fig. 8) appears to increase with
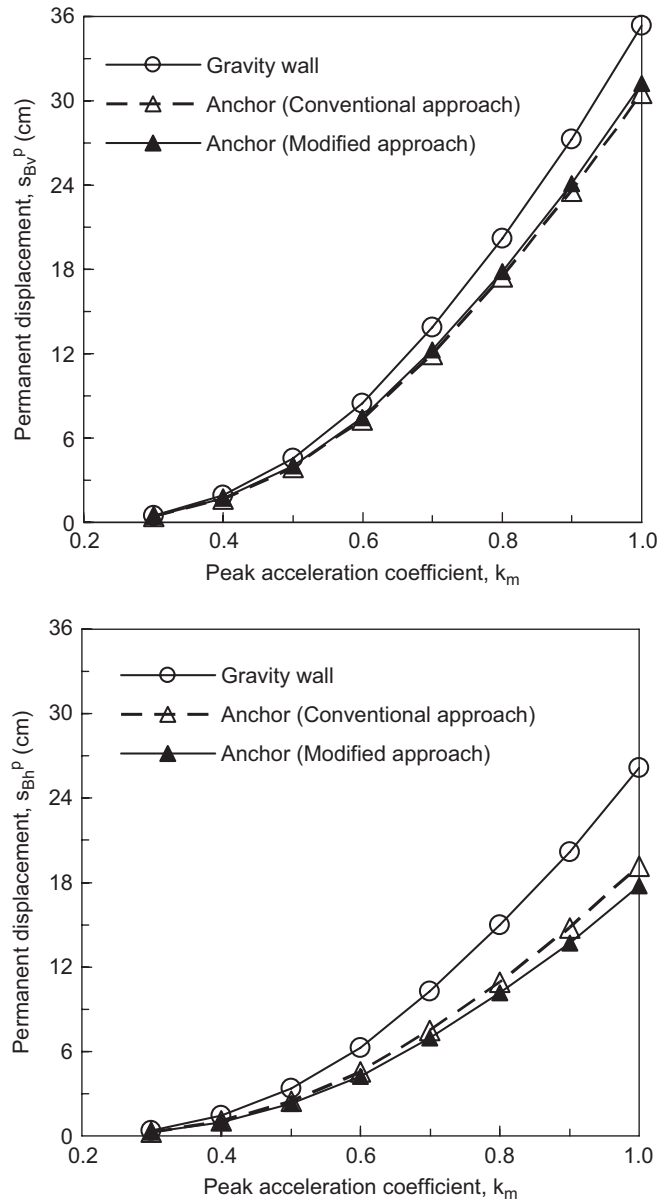
increasing peak earthquake acceleration, becoming significant for peak earthquake accelerations greater than 0.5g (Fig. 12). For the entire range of k_m values in Fig. 12, this difference translates into vertical and horizontal permanent displacements (s_{Bv}^p and s_{Bh}^p) of the anchor-reinforced slope (in the case of modified reinforcement approach) smaller by 12% and 32%, respectively, compared to the vertical and horizontal displacements on the top of the active wedge behind the gravity retaining wall.

5. Conclusions

A dynamic displacement analysis based on the sliding block concept was undertaken to investigate the seismic performance of a dry homogeneous fill slope supported by a gravity retaining wall or reinforced with anchors. Although both stabilizing techniques provided the same design yield coefficient for the sliding soil mass

within the fill material, in terms of seismic displacements, the fill stabilization method involving reinforcement with anchors appears to be more effective when compared to the gravity retaining wall. The main disadvantage of the gravity retaining wall lies essentially in its basic design principle, i.e., the weight of the wall, which provides most if not all of the resistance to sliding, but at the same time contributes indirectly to the amplification of the seismic displacements of the sliding soil mass through the wall inertia developed during the earthquake shaking. As demonstrated in this study, the superiority of anchors over gravity retaining walls becomes significant for peak earthquake accelerations greater than 0.5g suggesting that anchor systems may represent a better option to stabilize earth structures in areas prone to powerful earthquakes.

Acknowledgment

References

[1] Sidle RC, Kamai T, Trandafir AC. Evaluating landslide damage during the 2004 Chuetsu earthquake, Niigata, Japan. Eos Trans Am Geophys Union 2005;86(13). 133, 136.

[2] Kamai T, Trandafir AC, Murao H. Urban landslides induced by the 2004 Niigata-Chuetsu earthquake. In: Proceedings of the symposium on evaluation of seismic performance and safety of residential ground, Japan Geotechnical Society, 2005. p. 17–24.

[3] Newmark NM. Effects of earthquakes on dams and embankments. Géotechnique 1965;15(2):139–59.

[4] Franklin AG, Chang FK. Permanent displacement of earth embankments by Newmark sliding block analysis. Miscellaneous paper S-71-17. Vicksburg, MI: Soil and Pavements Lab, US Army Eng Waterways Expt Stn; 1977.

[5] Maksidi FI, Seed HB. Simplified procedure for estimating earth dam and embankment earthquake-induced deformations. J Geotech Eng, ASCE 1978;104(7):849–67.

[6] Trandafir AC, Sassa K. Seismic triggering of catastrophic failures on shear surfaces in saturated cohesionless soils. Can Geotech J 2005;42(1):229–51.

[7] Trandafir AC, Sassa K. Newmark deformation analysis of earthquake-induced catastrophic landslides in liquefiable soils. In: Proceedings of the 9th international symposium on landslides, Rio de Janeiro, vol. 1. Rotterdam: Balkema; 2004. p. 723–8.

[8] Trandafir AC, Sassa K. Evaluation of catastrophic landslide hazard on gentle slopes in liquefiable soils during earthquakes. In: Proceedings of the international conference on landslide risk management, Vancouver, Canada. Rotterdam: Balkema; 2005. p. 629–35.

[9] Chugh AK. Dynamic displacement analysis of embankment dams. Géotechnique 1995;45(2):295–9.

[10] Sarma SK. Stability analysis of embankments and slopes. Geotechnique 1973;23(3):423–33.

[11] Sarma SK. Seismic displacement analysis of earth dams. J Geotech Eng, ASCE 1981;107(12):1735–9.

[12] Ling HI, Leshchinsky D. Seismic performance of simple slopes. Soils Found 1995;35(2):85–94.

[13] Chang CJ, Chen WF, Yao JTP. Seismic displacements in slopes by limit analysis. J Geotech Eng, ASCE 1984;110(7):860–74.

[14] Seed HB, Goodman RE. Earthquake stability of slopes of cohesionless soils. J Soil Mech Found Div, ASCE 1964;90(6):43–73.

[15] Richards R, Elms DG. Seismic behavior of gravity retaining walls. J Geotech Eng Div 1979;105(4):449–64.

[16] Whitman RV, Liao S. Seismic design of retaining walls. Miscellaneous paper GL-85-1.Vicksburg, MI: US Army Eng Waterways Expt Stn; 1985.

[17] Kim SR, Jang IS, Chung CK, Kim MM. Evaluation of seismic displacements of quay walls. Soil Dyn Earthquake Eng 2005;25:451–9.

[18] Michalowski RL, You L. Displacements of reinforced slopes subjected to seismic loads. J Geotech Geoenviron Eng, ASCE 2000;126(8):685–94.

[19] Nadim F. A numerical model for evaluation of seismic behavior of gravity retaining walls. ScD thesis, Research report R82-33. Cambridge, MA: Department of Civil Engineering, Massachusetts Institute of Technology; 1982.

[20] Nadim F, Whitman RV. Seismically induced movement of retaining walls. J Geotech Eng, ASCE 1983;109(7):915–31.

[21] Kramer SL, Smith MW. Modified Newmark model for seismic displacements of compliant slopes. J Geotech Geoenviron Eng, ASCE 1997;123(7):635–44.

[22] Rathje EM, Bray JD. An examination of simplified earthquake-induced displacement procedures for earth structures. Can Geotech J 1999;36(1):72–87.

[23] Wartman J, Bray JD, Seed RB. Inclined plane studies of the Newmark sliding block procedure. J Geotech Geoenviron Eng, ASCE 2003;129(8):673–84.

[24] Kramer SL. Geotechnical earthquake engineering. Upper Saddle River, NJ: Prentice-Hall Inc.; 1996. pp. 653.

[25] GEO-SLOPE International Ltd. Computer program SLOPE/W for slope stability analysis. User's guide, version 2. Calgary, Alta., Canada, 1993.

[26] Okabe S. General theory on earth pressure and seismic stability of retaining wall and dam. Proc Jpn Soc Civil Eng 1924;10(6):1277–323.

[27] Mononobe N. Investigations on vertical ground motion and some related topics. Proc Jpn Soc Civil Eng 1924;10(5):1063–94.

[28] Seed HB, Whitman RV. Design of earth retaining structures for dynamic loads. Lateral stresses in the ground and design of earth retaining structures. New York: ASCE; 1970. p. 103–47.

[29] Wood JH. Earthquake-induced soil pressures on structures. Report no. EERL 73-05. Pasadena, CA: Earthquake Engineering Research Laboratory, California Institute of Technology; 1973.

[30] Wood JH. Earthquake-induced pressures on a rigid wall structure. Bull N Z Soc Earthquake Eng 1975;8(3):175–86.

[31] Steedman RS, Zeng X. The seismic response of waterfront retaining walls. In: Proceedings of the ASCE specialty conference on design and performance of earth retaining structures, Special Technical Publication 25. Ithaca, New York: Cornell University; 1990. p. 872–86.

[32] Cai F, Ugai K. Reinforcing mechanism of anchors in slopes: a numerical comparison of results of LEM and FEM. Int J Numer Anal Methods Geomech 2003;27:549–64.